PROTOSTELLAR WINDS AND CHONDRITIC METEORITES

Formation of Solids: The First Step

HSIEN SHANG[1], FRANK H. SHU[1], TYPHOON LEE[2], AND ALFRED E. GLASSGOLD[3]

[1]*Astronomy Department, University of California, Berkeley, CA 94720-3411, USA*
[2]*Institutes of Earth Sciences and Astronomy and Astrophysics, Academia Sinica, Nankang, Taipei 115, TAIWAN*
[3]*Physics Department, New York University, New York, NY 10003*

Received: 26 August 1999; Accepted: 17 December 1999

Abstract. We discuss the interaction between the magnetosphere of a young star and its surrounding accretion disk. We consider how an X-wind can be driven magnetocentrifugally from the inner edge of the disk where accreting gas is diverted onto stellar field lines either to flow onto the Sun or to be flung outwards with the wind. The X-wind satisfies many observational tests concerning optical jets, Herbig-Haro objects, and molecular outflows. Connections may exist between primitive solar system materials and X-winds. Chondrules and calcium-aluminum-rich inclusions (CAIs) experienced short melting events uncharacteristic of the asteroid belt where meteorites originate. The inner edge of the solar nebula has the shortest orbital timescale available to the system, a few days. Protosolar flares introduce another timescale, tens of minutes to hours. CAIs may form when solids are lifted from shaded portions of the disk close to the Sun and are exposed to its intense light for a day or so before they are flung by the X-wind to much larger distances. Chondrules were melted, perhaps many times, by flares at larger distances from the Sun before being launched and annealed, but not remelted, in the X-wind. Aerodynamic sorting explains the narrow range of sizes with which CAIs and chondrules are found in chondritic meteorites. Flare-generated cosmic-rays may induce spallation reactions that produce some of the short-lived radioactivities associated with primitive solar system rocks.

Keywords: X-wind, Young Stellar Objects, Jets; Chondrules, CAIs, Extinct Radioactivities

1. Introduction

Together with comets, chondritic meteorites are among the most primitive material in the solar system. They contain spherically shaped particles, chondrules and refractory inclusions (CAIs), indicating that they solidified from a molten state, juxtaposed with matrix material that never experienced high temperatures. Such a mixture cannot be naturally explained by formation near the location of the parent bodies of meteorites in the asteroid belt. The high abundance of igneous rocks in chondritic meteorites implies that large reservoirs of material in the early solar system experienced efficient thermal processing. We propose that chondritic meteorites arise as a byproduct of the most energetic phase of protostellar evolution, through gas-solid coupling during bipolar outflows.

During the formation of a sunlike star, a wind can emerge from the innermost part of a rapidly rotating circumstellar disk that interacts with the strong magnetic field of the central star (Shu *et al.*, 1994a; 1994b; Shang and Shu, 1999). This wind collimates to a jet and drives a bipolar molecular outflow in the surrounding gas (Shu *et al.*, 1995). The rotating, outwardly blowing, gas flings solids like stones

Space Science Reviews **92:** 153–176, 2000.

from a sling out of the cool disk. Rocks lifted from the shaded disk close to the Sun by the wind are exposed to full sunlight for a day or so, melting and resolidifying to become CAIs (Shu *et al.*, 1996). Rocks farther from the Sun are heated less intensely by sunlight when lifted by the X-wind, but they may have become chondrule-like in previous melting episodes when bombarded and heated by protosolar flares (Shu *et al.*, 1997; Lee *et al.*, 1998). Mm- to cm-sized objects fall back to the disk at interplanetary distances, where they accumulate along with the ambient cold dust in the solar nebula to form larger solid objects that are the parent bodies of chondritic meteorites. Smaller particles are carried to interstellar space, while larger ones fall out of the X-wind close to the launch radius and are eventually swept into the Sun by the general accretion flow in the disk. By such processes planetesimals can accumulate largely from igneous rocks of narrow size range, in contrast to conventional scenarios which predict that they should be made mostly from amorphous loosely aggregated solids (*e. g.*, Weidenschilling and Cuzzi, 1993).

The plan of this article is as follows. We first review the observations of jets and outflows from low-mass young stellar objects (YSOs) to establish the basic astrophysical context. We then discuss the X-wind theory that has been developed by our group to explain these observations. We finally consider the implications of this picture for solids that are exposed to the energetic environment associated with X-winds and show that they provide a natural and simple explanation for many of the puzzles long attached to the existence of CAIs and chondrules in chondritic meteorites.

2. Winds, Jets and Bipolar Outflows

The discovery of energetic jets (Bok, 1978; Cudworth and Herbig, 1979) and bipolar molecular outflows (Snell *et al.*, 1980; Rodríguez *et al.*, 1980) from YSOs marks an important breakthrough in astronomers' understanding of the evolution of low-mass stars. The frequent association of jets and outflows with young stars suggests that all YSOs go through a period of heavy mass loss before reaching the main sequence (Bally and Lada, 1983; Cabrit and Bertout, 1992; Edwards and Snell, 1982; Fukui *et al.*, 1993; Lada, 1985; Margulis and Lada, 1985).

Observations of the outflow phenomena cover a wide range of wavelengths, from the ultraviolet to the radio, and involve ionized, atomic and molecular gas in various excitation states. Molecular outflows are usually traced by CO molecules as bipolar lobes of gas containing both fast moving and swept-up material. The morphology suggests that an underlying wind drives the outflow. Shock-excited nebulosities, the Herbig-Haro (HH) objects discovered independently by Herbig (1950; 1951) and Haro (1952; 1953), demarcate the brightest portions of optical jets that sometimes lie along the central axis of the cavities of the bipolar lobes.

Jets observed with the Hubble Space Telescope (HST) display high degrees of collimation. Their HH objects emit in permitted transitions of atomic hydrogen, as a recombination cascade from ionized states, and in forbidden transitions of [OI], [NII], and [SII], which are species whose low-lying electronic levels are easily

excited by collisional impact with thermal electrons. Cudworth and Herbig (1979) first established that HH objects have large proper motions by showing that HH 28 and HH 29 in the dark cloud L1551 move across the sky at speeds of $\sim$150 km/s along trajectories that trace back to an embedded infrared source IRS 5 discovered by Strom *et al.* (1974). Somewhat larger values, 200–300 km/s, are now known to typify the space velocities of most YSO jets.

CO linewidths of the order of 10 km/s in the L1551 region had been found earlier (Knapp *et al.*, 1976), and Strom *et al.* (1974) deemed such linewidths too large to be due to gravitational collapse, suggesting instead that a powerful stellar wind might generate the disturbance. Snell *et al.* (1980) mapped the CO emission in L1551 region and found the high-velocity CO to form bipolar lobes moving in opposite directions from IRS 5. They proposed that a bipolar stellar wind of 100–200 km/s from IRS 5, as tracked by HH 28/29, is sweeping up ambient molecular cloud gas into two thin shells that move in opposite directions at $\pm$15 km/s before projection along our line of sight. Later observations showed that the two HH objects are simply the most prominent knots of optical emission in a more continuous flow of the part of the jet that points out of the cloud toward us (Mundt and Fried, 1983; Reipurth, 1989). Further mapping of the thermal free-free emission at radio wavelengths, which does not suffer extinction by interstellar dust, showed ionized gas in the form of a smaller two-sided jet centered on IRS 5 (Bieging *et al.*, 1984).

What drives molecular outflows? Do jets operate alone? If we count only the ionized component of YSO jets, they contain insufficent momentum to drive the surrounding CO gas. Moreover, molecular outflows are typically far less well collimated than optical and radio jets. These deficiencies motivated Lizano *et al.* (1988), Giovanardi *et al.* (1992), Rodríguez *et al.* (1990), and Ruiz *et al.* (1992) to look for a neutral component to the winds from YSOs that drive molecular outflows. They succeeded in finding such neutral winds in the form of very broad line wings extending to 100 km/s and larger in the emission of the 21 cm line of atomic hydrogen toward the sources HH 7-11, L1551, and T Tau. The deduced mass loss rates of 10^{-6} to 10^{-5} $M_{\odot}$ yr^{-1} are comparable to the inferred accretion and infall rates of these young stars (Shu *et al.*, 1987). Although atomic hydrogen winds have only been directly observed in a few sources because of sensitivity difficulties in making the measurements, all astronomers now believe that YSO winds and jets are only lightly ionized, with the bulk of the momentum flux being carried in a neutral component. It is still controversial whether the atomic hydrogen is dissociated gas from ambient molecular hydrogen entrained by the jet or part of a wide-angle wind that accompanies a narrow core that appears as the optical jet. Our group prefers the latter association because it is difficult otherwise to understand how narrow jets can drive rather poorly collimated molecular outflows. Indeed, many images show non-precessing optical jets emerging along the central axes of biconical reflection nebulae (HH 34, Bührke *et al.*, 1988; 1548C27, Mundt *et al.*, 1984; Z CMa, Poetzel *et al.*, 1989; L1551 IRS 5, Stocke *et al.*, 1988) and the cavities of these biconical nebulae are too wide to be simply explained by anything other than a wide-angle wind.

2.1. Different Classes of Theoretical Models

All viable methods of driving YSO winds postulate a combination of rapid rotation and strong magnetic fields. Two classes of models involving hydromagnetic acceleration in centrifugally supported disks are currently popular. They differ in the origin of the magnetic field, and in whether the region of disk that feeds the wind spans a broad or narrow range of radii. The first class of models invokes large-scale magnetic fields, perhaps dragged in from the interstellar medium as part of the star-formation process, threading through extended regions of a disk undergoing Keplerian rotation (see the review of Königl and Pudritz, 2000). Such models are known generically as "disk winds," and their roots trace back to the seminal work of Blandford (1976) and Lovelace (1976). The second class of models invokes the strong magnetic field of the central star to truncate an electrically conducting accretion disk and to drive magnetocentrifugally both an outwardly flowing wind and an inwardly flowing funnel flow from a narrow zone (the X-region) near the disk's inner edge (see the review of Shu *et al.*, 2000). Such models are known as "X-winds," and their roots trace back to the seminal work of Mestel (1968) and Ghosh and Lamb (1979ab). X-winds arise from a narrow region around $R_{\rm X} \sim 0.04$ AU (*cf.* Sect. 3.1), whereas disk wind models cover a large range of radii from $\sim$0.04–100 AU. Only the X-wind processes enough rocky material at high temperatures and rapid timescales to provide a viable mechanism for making CAIs and chondrules; consequently, we focus on X-winds for the discussion of this article.

3. Star-Disk Interaction

In the X-wind model, the combination of strong magnetic fields and rapid rotation of the young star-disk system acts as an "eggbeater" to whip out part of the material from the surrounding disk while allowing the rest to sink deeper in the bowl of the gravitational potential well (an analogy suggested by G. Basri, personal communication). X-winds emerge from a narrow range of radii comparable to the vertical scale height near the inner edge of the disk (Shu *et al.*, 1994a), and they subsequently expand to become a space-filling wide-angle wind, whose high-density central core has the appearance of a well-collimated optical jet (Shu *et al.*, 1995; Shang *et al.*, 1998).

3.1. The X-Geometry

When a young star's magnetosphere interacts with its adjoining accretion disk, the gaseous disk will be truncated by the magnetic field at a radius $R_{\rm t}$ given by dimensional argument as

$$R_{\rm t} = \alpha_{\rm t} \left(\frac{\mu_*^4}{G M_* \dot{M}_{\rm D}^2} \right)^{1/7} , \tag{1}$$

constructed with the gravitational constant G, mass of the star M_*, disk accretion rate $\dot{M}_{\rm D}$, magnetic dipole moment of the star μ_*, and a coefficient α_t of order unity

to be discussed later. It is further convenient to define a radius R_X where the natural Keplerian angular velocity of the disk,

$$\Omega_X = \sqrt{\frac{GM_*}{R_X^3}} \tag{2}$$

equals the angular velocity of the star Ω_*. The effective potential (centrifugal plus gravitational) associated with a frame of reference that rotates at Ω_X is

$$V_{eff} = -\frac{GM_*}{(\varpi^2 + z^2)^{1/2}} - \frac{1}{2}\Omega_X^2 \varpi^2 + \frac{3}{2}\Omega_X^2 R_X^2. \tag{3}$$

In this paper, we shall use (ϖ, ϕ, z) to denote cylindrical coordinates, and (r, θ, ϕ) to denote spherical polar coordinates, both of which have origins at the center of the star. The arbitrary constant in the definition of potentials has been chosen for convenience to make $V_{eff} = 0$ at the X-point: $\varpi = R_X$ and $z = 0$. From Eqs. 2 and 3, we can show that the effective gravitational field also vanishes at the X-point, *i. e.*, $-\nabla V_{eff} = 0$ at $\varpi = R_x$ and $z = 0$. In fact, the X-point lies at a saddle of the effective potential, *i. e.*, at $\varpi = R_x$ and $z = 0$ we have

$$\frac{\partial^2 V_{eff}}{\partial \varpi^2} < 0, \quad \frac{\partial^2 V_{eff}}{\partial z^2} > 0.$$

Consequently, a contour plot of V_{eff} demonstrates that the critical equipotential surfaces intersect in an X-configuration at $\varpi = R_X$ and $z = 0$, which gives the X-point and the X-wind their names (Shu *et al.*, 1994b). In the meridional plane (ϖ, z), both the left and right sides of X make a 60° angle with the upper and lower surfaces of a flat horizontal disk (see Fig. 1, which shows the upper part of the X). The outer branches of the X turn asymptotically parallel to the z-axis at a distance $\varpi = 3^{1/2} R_X$. The inner branches intersect with the z-axis at a distance $z = \pm(2/3) R_X$ and wrap around the star to reintercept the disk at the X-point on the other side. The gravitational potential dominates to the left (funnel zone) and the centrifugal potential dominates to the right (wind zone); in these two sectors, V_{eff} becomes more negative and the material can flow "downhill" toward or away from the star. The top and bottom sectors of the X form the "uphill" directions of the saddle of the effective potential, and material from the disk cannot freely flow into these regions (dead zone).

By definition, magnetic fields are not strong enough to truncate the disk until R_t. The weaker field lines which would otherwise be threading through the disk outside of R_t are swept in by the accretion flow to get trapped there in a small fractional neighborhood ϵ of R_t (see below), building up strength until they can resist further compaction by the incoming disk accretion. If R_t is initially larger than R_X, then $\Omega_t < \Omega_X \equiv \Omega_*$, and, given enough time, field lines connecting the star and the disk will slow down the angular rotation rate of the star and bring R_X outward to equal R_t within order ϵ. If R_t is initially smaller than R_X, then $\Omega_t > \Omega_X \equiv \Omega_*$, and, given enough time, field lines connecting the star and disk will speed up the angular ro-

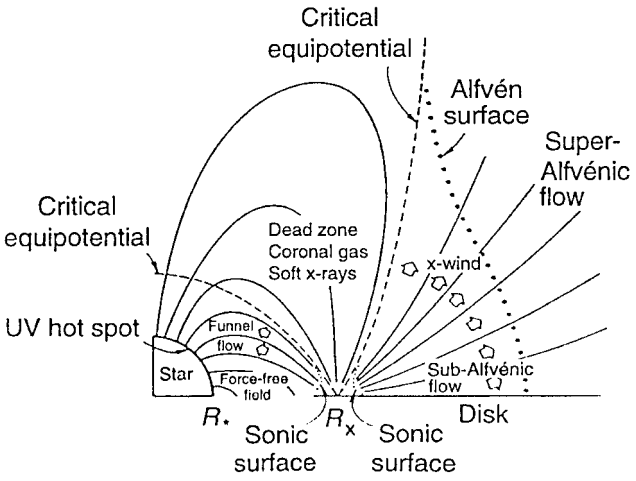

Figure 1. Schematic picture of the steady-state X-wind with closed dead zone (from Shu *et al.*, 1995).

tation of the star and bring R_X inward to equal R_t within order ϵ. In other words, in quasi-steady-state, we expect the star to corotate with the inner edge of the gaseous accretion disk; otherwise the field lines would suffer continuous wrapping into trailing or leading spirals whose back reaction on the system would cure the difficulty.

We now try to understand why field lines connecting the star and disk are trapped in a small region (X-region) of fractional size ϵ near the edge of the disk $R_t = R_X$. In the inner portion of the X-region, the gas is forced by the strong magnetic fields to rotate slightly slower than its natural Keplerian rate; thus, this gas loses angular momentum and falls in a funnel flow toward the star (Ostriker and Shu, 1995). In the outer portion of the small X-region, the gas is forced by the strong magnetic field to rotate slightly faster than its natural Keplerian rate; thus, this gas gains angular momentum and is flung outwards in a magnetocentrifugally driven wind. The back reaction on the gas remaining in the X-region – which requires loss of angular momentum in the outer parts and gain of angular momentum in the inner parts – is to pinch the gas and the fields to which they are approximately tied on both sides toward the middle. This pinch is what leads to the geometry of trapped flux that is displayed in Figs. 2 and 3.

The quantity ϵ equals the ratio of the isothermal sound speed a_X to the orbital velocity $R_x\Omega_x$ at the X-point; it has a typical value, 0.03, which is quite small compared to unity (Shu *et al.*, 1994a). To derive this result, notice that gravity and centrifugal acceleration balance exactly at R_X. The X-region is defined by a size where magnetic fields are strong enough to enforce uniform rotation at angular speed Ω_X and give gas excess speeds or deficits relative to Keplerian that are of the order of the sound speed a_X. When the gas is within a small radial distance $\Delta\varpi$, positive or negative, from R_x, the excess or deficit of centrifugal acceleration is of order $\Omega_X^2\Delta\varpi$. Within a sound crossing time $\Delta\varpi/a_X$, the excess acceleration can yield differential fluid speeds $\sim a_X$ if

$$(\Omega_X^2\Delta\varpi)(\Delta\varpi/a_X) \sim a_X. \tag{4}$$

Solving for $\Delta\varpi$ yields $\Delta\varpi \sim \pm(a_{\rm X}/\Omega_{\rm X})$, *i.e.*,

$$\frac{|\Delta\varpi|}{R_{\rm X}} \sim \frac{a_{\rm X}}{R_{\rm X}\Omega_{\rm X}} \equiv \epsilon, \tag{5}$$

which shows that the width of the X-region is of order $\epsilon R_{\rm X}$.

3.2. X-WIND, FUNNEL FLOW, AND THE DEAD ZONE

In steady state, the coefficient in the formula for the disk truncation radius $R_{\rm t} = R_{\rm X}$ is given by a calculation by Ostriker and Shu (1995):

$$\alpha_{\rm t} = \Phi_{{\rm d}x}^{-4/7}, \tag{6}$$

where $\Phi_{{\rm d}x}$ is a nondimensional measure of the unperturbed dipole flux at the X-point. In a model with closed dead zone field lines, $\Phi_{{\rm d}x} = 2\bar{\beta} f^{1/2}$, with the symbols $\bar{\beta}$ and f to be described below. It is convenient to nondimensionalize all other quantities by using the units:

$$R_{\rm X},\ \Omega_{\rm X} R_{\rm X},\ \dot{M}_{\rm w}/4\pi R_{\rm X}^3\Omega_{\rm X},\ (\Omega_{\rm X}\dot{M}_{\rm w}/R_{\rm X})^{1/2}, \tag{7}$$

for length, velocity, density and magnetic field (Shu *et al.*, 1994b). If we know the input parameters: mass of the star M_*, radius of the star R_*, disk accretion rate $\dot{M}_{\rm D}$, and the magnetic dipole moment of the star μ_*, the theory predicts all other numbers for comparisons with observations.

For magnetic fields strong enough to truncate the disk at an inner edge of radius $R_{\rm X} > R_*$, a wind outflow and a funnel inflow are launched magnetocentrifugally from the X-region. The mass loss rate in the wind $\dot{M}_{\rm w}$ and the mass accretion rate onto the star $\dot{M}_*$ are related to the disk accretion rate $\dot{M}_{\rm D}$ by

$$\dot{M}_{\rm w} = f\dot{M}_{\rm D}, \qquad \dot{M}_* = (1-f)\dot{M}_{\rm D}, \tag{8}$$

where

$$f = \frac{1-\tau-\bar{J}_*}{\bar{J}_{\rm w}-\bar{J}_*}, \tag{9}$$

is determined by angular momentum balance in the X-region (Shu *et al.*, 1994a; Ostriker and Shu, 1995). Averaged over all streamlines, $\bar{J}_{\rm w}$ and $\bar{J}_*$ are the dimensionless specific angular momenta carried by matter and field in the wind and the funnel flow, respectively; and τ is the dimensionless viscous torque exerted on the X-region by disk material external to it. If we assume that the near-uniform rotation of the X-region makes $\tau \approx 0$, and if we assume that the net specific angular momentum deposited into a small star $\bar{J}_* \approx 0$, we have $f \approx 1/\bar{J}_{\rm w}$. This formula can be used to determine either f from $\bar{J}_{\rm w}$ or $\bar{J}_{\rm w}$ from f. We do the latter here.

The fraction f of the matter accreting in the disk that climbs onto stellar field lines which lead to X-wind outflow versus the fraction $(1-f)$ that climbs onto stellar field lines which lead to funnel inflow should be obtained, in principle, by a calculation of how lightly ionized gas in the X-region diffuses onto such field lines. Lack-

ing such a detailed calculation, which is very complex (see the discussion in Shu *et al.*, 1994a), we may nevertheless make an educated guess. Field lines are tightly bunched in the X-region, and matter slowly and turbulently accreting through the disk probably has an equally good chance to attach to any third of the trapped flux in the wind zone, dead zone, and funnel zone. However, gas that attaches to the dead zone field lines have nowhere to go dynamically except to systematically wander inwards to the funnel zone. This simple analysis suggests that $f \approx 1/3$ and $(1-f) \approx 2/3$. For $f/(1-f) \approx 1/2$, to make a slowly-rotating $1\,M_\odot$ star requires the X-wind to blow away $0.5\,M_\odot$ of material that carries away the excess angular momentum of inner disk accretion. The streamline-averaged terminal velocity of such a wind equals $(2\bar{J}_{\rm w} - 3)^{1/2} R_{\rm X}\Omega_{\rm X}$ (see Eq. 18). The quantity $\bar{J}_{\rm w} \approx 1/f \approx 3$; therefore, we expect a wind terminal speed $\approx \sqrt{3}$ times the orbital speed $R_{\rm X}\Omega_{\rm X}$ of the inner edge of the disk. Thus, X-winds are highly efficient in turning around the mass infall of collapsing cloud cores. For each gram of matter accumulated by a forming star, approximately half a gram is flung back out to molecular clouds at 200–300 km/s. X-winds are indeed powerful drivers of bipolar outflows!

The basic energy reservoir of the steady-state system is the gravitational potential energy of accreting matter, with viscous and magnetic torques acting merely as intermediaries to tap into this reservoir (see Shu *et al.*, 1995). When the funnel stream impacts the star, dissipation of kinetic energy in the hot spots creates a radiative luminosity:

$$L_{\rm hot} = (1-f)\frac{GM_*\dot{M}_{\rm D}}{R_*}\left(1 + \frac{R_*^3 \sin^2\theta_{\rm h}}{2R_{\rm X}^3} - \frac{3R_*}{2R_{\rm X}}\right), \tag{10}$$

where $\theta_{\rm h}$ is the mean colatitude of the hot spot measured from the pole (Ostriker and Shu, 1995). For a star of radius $R_*/R_{\rm X} = 0.25$, the funnel flow strikes the star surface at colatitudes $30^\circ \le \theta \le 37.8^\circ$ (Ostriker and Shu, 1995). These hot spots are sources of ultraviolet photons. For $R_* \ll R_{\rm X}$, the accretion luminosity approaches the naive expression $(1-f)GM_*\dot{M}_{\rm D}/R_*$, but when $\theta_{\rm h}$ moves to the equator ($\theta_{\rm h} = \pi/2$) for $R_{\rm X} \to R_*$, $L_{\rm hot}$ approaches zero.

In the corotating frame of $\Omega_{\rm X} = \Omega_*$, gas loads onto field lines in the X-region and separates at the extremes into two flows, to be either funneled onto the star at the hot spots or launched into an X-wind. The funnel flow occurs on distorted dipole field lines that close above and below the equator of the star (see Fig. 2). The wind flow occurs on field lines rooted in the midplane of the disk and open from there to the interstellar medium. These are one-half of the closed dipole field lines that once threaded from one hemisphere of the star through the disk and returned back to the star in the other hemisphere, but they have since been opened by the ram pressure of the X-wind (for a time-dependent simulation of this process, see Hayashi *et al.*, 1996). The other half of the dipole-like field have become open lines with one end attached to the upper or lower hemisphere of the star and with the other end stretched toward interstellar space (Ostriker and Shu, 1995). They eventually

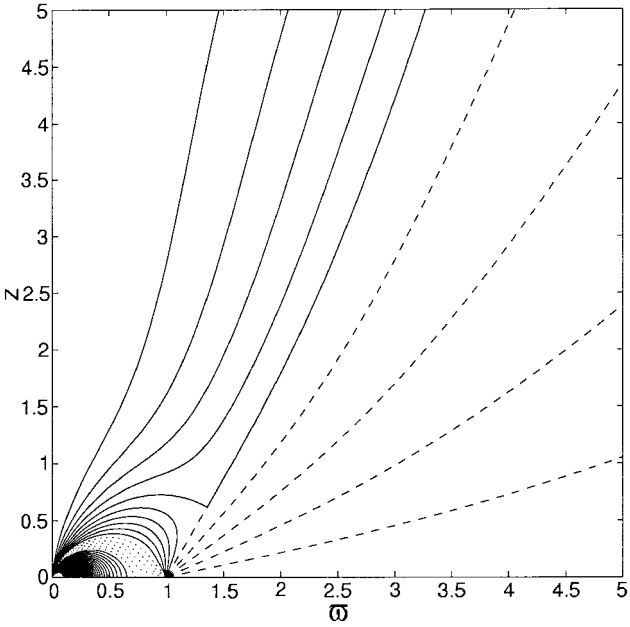

Figure 2. The poloidal magnetic field configuration resulting from an actual self-consistent calculation (Ostriker, Shang, and Shu, unpublished) that imposes approximate pressure balance across the interfaces of the funnel flow (*dotted curves*), dead zone (*solid curves*), and X-wind (*dashed curves*). Also denoted by solid curves are stellar field lines opened by the X-wind (*i. e.*, those that connect at infinity to the dashed lines in the X-wind) and virtually unperturbed dipole field lines that are rooted in the star. Adapted from Shu *et al.* (1999).

join with the X-wind field lines from the disk, but we refer to both as "opened" field lines since the joining formally occurs at infinity in steady state models.

The middle portion of the magnetic flux trapped in the X-region contains dead-zone field lines as shown in Fig. 2. These field lines are loaded only with coronal gas heated by transient magnetic activity, and not with cool dense material originally from the disk. The dead-zone field lines may be either open or closed, depending on the level of activity in the corona relative to the strength of the magnetic field in the dead zone. Figure 2 illustrates a computed example where the dead zone fields are assumed to be closed, maintaining pressure equilibrium with the first streamline of the funnel flow and the last streamline of the X-wind. A bifurcation in the behavior of field lines occurs on a separatrix. Below the separatrix, the surface that separates regions with opposing magnetic fluxes, the X-wind abuts the dead zone, whereas above the separatrix, the X-wind abuts opened stellar field lines that provide a hollow core (filled with coronal gas) to the X-wind. The interface below the separatrix has poloidal field lines pointing all in the same direction, but the interface above the separatrix forms a surface of reversed poloidal field called a helmet streamer in solar physics. When the dead zone is closed and we ignore any fields unassociated with the star originally, the X-wind contains an exactly equal amount (but opposite in sign) of magnetic flux as the axially directed stellar field lines in the hollow core. This must be true since the two sets of fields connect, line by line, at infinity.

When the dead zone is open, say, because of coronal mass ejections (CMEs), a helmet streamer geometry develops for the dead zone itself (see Fig. 3). Equal and opposite signs of the magnetic flux across the helmet streamer arise that correspond to stellar field lines opened not by the X-wind, but by the coronal mass ejections.

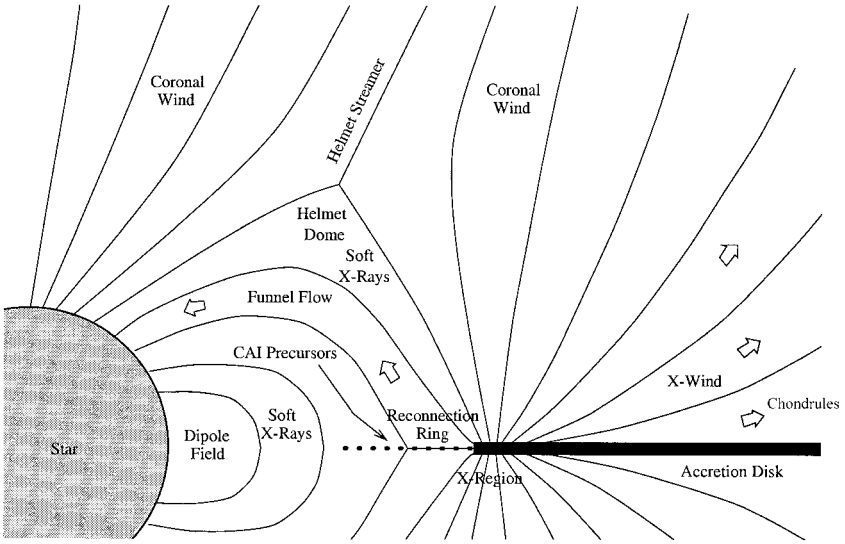

Figure 3. Schematic picture of the general X-wind with open dead zone.

The maximum hollow core occurs when all of the dead zone field lines are opened; in this case, the hollow core contain equal contributions from stellar field lines opened by the X-wind, stellar field lines opened by the CMEs, and disk field lines in the dead zone opened by the same CMEs. The X-wind now contains one third as many field lines as those in the hollow core filled with coronal gas.

In a time-dependent environment, we may envisage the X-wind outflow and funnel inflow to occur against a backdrop where the dead zone fluctuates, at its extremes, between completely closed and completely open geometries. These changes might occur in response to magnetic cycles such as those seen in the modern Sun. Magnetic cycles may also underlie the phenomenon of "pulsed jets," whereby quasi-periodic variations of the jet speed or mass-loss-rate lead to bisymmetric strings of HH objects spaced perhaps a decade or so apart. The inner edge R_X will fluctuate about its equilibrium position in these circumstances (Shu *et al.*, 1997). During the low states of magnetic cycles, the accretion disk can intrude farther inward into a weaker magnetosphere. The star has too much inertia to increase its angular rotation rate to match Ω_t on a decade-like timescale, so the star and the funnel field lines attached to it will rotate slower than the inner edge of the gaseous disk, $\Omega_* < \Omega_t$. These circumstances will aid the funnel flow, but a reduced X-wind outflow can still occur as long as the disk's inner edge continues to contain trapped flux and rotates at Keplerian speeds. Indeed, reductions in f and R_t will favor larger terminal velocities for the X-wind. In high magnetic states, the stronger magnetosphere will push R_t to larger values, with the consequence that the star will rotate faster than the inner edge of the accretion disk, $\Omega_* > \Omega_t$. These circumstances will impede funnel flow, and the increases in f and R_t will favor lower terminal velocities of the X-wind.

Consider now the effect of these fluctuations for magnetic flares. When field lines have bifurcations of a Y shape, such as in a helmet streamer, a current sheet extends from the crotch of the Y to infinity because of the oppositely directed (poloidal) field lines on either side of the helmet streamer. A similar change of magnetic topology exists at the base of the funnel flow, in the so-called "reconnection ring," where dipole-like field lines from the star bifurcate in behavior between making an excursion to be trapped in the x-region and crossing the midplane of the system without making this back-and-forth excursion (Ostriker and Shu, 1995). In a situation with nonzero electrical resistivity (*i. e.*, nonideal MHD), the large currents carried in the sheets of oppositely directed fields will dissipate, causing the fields to reconnect and change their topology (to a more dipole-like configuration). Empirically, in the case of the modern Sun, the reconnection events often occur not with a slow and steady release of energy, but explosively, in tens of minutes to hours. Recovery of the pre-flare configuration depends on the presence of differential rotation to resume stressing the magnetic fields.

If low-mass protostars behave analogously to the modern Sun, we may expect two kinds of flare events to arise when magnetic field configurations are kept in a state of disequilibrium by differential fluid motions (Linker and Mikić, 1995): Gradual flares, occurring on a timescale of hours to days, arise in coronal mass ejections when differential rotation wraps up closed field lines, increasing the magnetic stresses until they blow open some of the offending closed field lines, in the process, ejecting coronal matter via strong shockwaves. Impulsive flares, lasting tens of minutes to hours, arise in magnetic reconnection events when oppositely directed field lines created by other processes (*e. g.*, CMEs or flux trapping in the X-region) annihilate explosively, releasing copious magnetic energy that accelerates ambient particles to cosmic-ray energies.

Astrophysical evidence that such events are present in young low-mass stars to a much greater degree than the modern Sun include the spectral line profiles that vary from night to night in T Tauri stars (TTSs), the ubiquity of X-ray flares in TTSs and protostars lasting from tens of minutes to hours to days, and the aforementioned quasi-periodicities on decades kind of timescales inferred for pulsed YSO jets. Indeed, recent satellite measurements from ASCA show that the X-ray emission from embedded protostars has a hard component that is missing or weaker in classical TTSs (TTSs with accretion disks) and weak-lined TTSs (TTSs without accretion disks). The X-ray emission becomes harder and stronger during flares, consistent with our interpretation that an extra component to the usual coronal activity associated with strong stellar magnetic fields is present when a vigorously accreting disk is added to the problem (see the review of Glassgold *et al.*, 2000).

Because solids are imperfectly coupled to gas and may either drop out of the funnel flow or drift slowly inward relative to rotating layer of gas, rocky material may orbit in a flattened distribution interior to the inner edge of the gas disk (see Fig. 3). Under plasma drag with a slowly rotating corona, this tongue of extruded dust may keep spiraling closer to the Sun until the temperature reaches a high enough value

to evaporate even the most refractory of solar system materials. This inference is consistent with observations that suggest optically thick, YSO dust disks often come within 0.5 R_X of their central stars (Meyer *et al.*, 1997). Thus, the extruded tongue of dust, unshielded by the usual complement of hydrogen and helium gas, constitutes an attractive environment for making CAIs, when we consider the nuclear reactions that can be induced by flare-generated cosmic-ray particles in the reconnection ring. Transport of this heated and irradiated material to interplanetary distances can occur if fluctuations in the launch point for X-winds cause R_X to migrate inwards to regions previously occupied by the protoCAIs and the reconnection ring. In such a picture, it is tempting to try to make chondrules via impulsive flare-heating at larger distances from the Sun and to fling such rocks out via the X-wind before they have had a chance to enter very deeply into the reconnection ring.

4. X-wind as a Jet-Bearing Inner Disk Wind

The acceleration of the X-wind by transsonic flow in the X-region occurs by a combination of gas pressure and magnetic forces. Past the sonic (or slow-MHD) transition, magnetic forces continue to accelerate the X-wind from sub-Alfvénic to super-Alfvénic and super-fast-MHD speeds. Provided the speeds reached at the last transition-surface are larger than the escape speed from the system, the gas will flow to the interstellar medium at some nonzero terminal velocity. Once the gas begins to flow at hypersonic speeds, we may ignore the role of a finite sound speed, and take the limit $\epsilon \to 0$. Bernoulli's equation (BE), which holds in the corotating frame even for a magnetized medium, then implies

$$\frac{1}{2}|\mathbf{u}|^2 + \mathrm{V}_{\mathrm{eff}} = \text{const along a streamline.} \tag{11}$$

The constant of integration may be evaluated to be zero (to order ϵ^2) since $|\mathbf{u}|$ and V_{eff} both vanish at the X-point. At large distances, the asymptotic form of the above equation becomes, in a nonrotating frame of reference, $v_{\mathrm{w}} = (2J_g - 3)^{1/2} R_{\mathrm{X}} \Omega_{\mathrm{X}}$, where v_{w} is the terminal velocity of the wind and $J_{\mathrm{g}} = \varpi v_\varphi / R_{\mathrm{X}}^2 \Omega_{\mathrm{X}}$ is the dimensionless specific angular momentum of the gas. Since the total specific angular momentum carried in the gas J_{g} is less than the total specific angular momentum carried by the gas and Maxwell torques, $J = J_{\mathrm{g}} + J_B$, the streamline-averaged terminal velocity reached by the X-wind satisfies $\bar{v}_{\mathrm{w}} \leq (2\bar{J} - 3)^{1/2} R_{\mathrm{X}} \Omega_{\mathrm{X}}$. It turns out that the inequality applies for flows that fail to make a fast-MHD transition ("breeze solutions"), while the equality applies for flows that do become super-fast-MHD ("wind solutions"). The latter are the ones of interest to us, because the partial differential equation (PDE) that breeze solutions satisfy is elliptic in character out to infinity, and this requires an artificial imposition of outer boundary conditions that nature probably cannot supply.

The full mathematical formulation of the X-wind is given by Shu *et al.* (1994b). It contains a set of conservation laws coupled to a second-order PDE for the stream

function $\psi(\varpi, z)$, commonly known as the Grad-Shafranov equation (GSE). The stream function is related to the fluid velocity in the meridional plane by

$$\mathbf{u}_p = \frac{\mathbf{e}_\varphi}{\varpi\rho} \times \nabla\psi. \tag{12}$$

Loci of ψ =constant defines the streamlines in the (ϖ, z) plane and label, in a certain nondimensionalization the fraction of the mass flux carried by the axisymmetric flow after an integration over the azimuthal angle ϕ. Thus, $\psi = 0$ and $\psi = 1$ define the lower and upper boundaries of the flow in the meridional plane. Solving the GSE, which is a PDE of mixed elliptic and hyperbolic type for "wind solutions," is extremely difficult; but Najita and Shu (1994) did succeed in finding good numerical solutions in the main acceleration region of the flow below the Alfvén crossing.

Fortunately, the GSE can be solved analytically in two asymptotic regimes, near to the x-point and far from it. Because of the smallness of ϵ, the flow emerges from the x-point in the near regime as a fan of streamlines (Shu *et al.*, 1994b):

$$\vartheta(\psi) = \frac{\pi}{3\bar{\beta}} \int_0^\psi \beta(\psi)\, d\psi, \qquad \text{with} \qquad \bar{\beta} \equiv \int_0^1 \beta(\psi)\, d\psi, \tag{13}$$

where ϑ is the angle with respect to the ϖ axis with vertex at the X-point, $\beta(\psi)$ is the ratio of magnetic field to mass flux (*i. e.*, it describes how mass is loaded onto field lines), and $\vartheta = \pi/3$ (*i. e.*, 60°) is the locus of the $\psi = 1$ streamline. In the far regime, we have a parametric representation of the X-wind streamlines. For the case of closed dead-zone fields, we require magnetic pressure balance across the interface between open stellar fields B_z and wind fields that are dominated asymptotically by the toroidal component B_φ. With one parameter C, which corresponds to the dimensionless axial current needed to support B_φ in the X-wind, curves in $r - \theta$ space for given ψ's are generated by (see the derivation in Shu *et al.*, 1995):

$$r = \frac{2\bar{\beta}}{C} \cosh[F(C, 1)], \tag{14}$$

and

$$\theta = \sin^{-1}\{\mathrm{sech}[F(C, \psi)]\}, \tag{15}$$

where

$$F(C, \psi) \equiv \frac{1}{C} \int_0^\psi \frac{\beta(\psi) d\psi}{[2J(\psi) - 3 - 2C\beta(\psi)]^{1/2}}. \tag{16}$$

When the field lines of the dead zone are completely open, $6\bar{\beta}$ replaces the factor $2\bar{\beta}$ in Eq. 14, because there are then three times as many field lines in the hollow core for the toroidal field of the X-wind to confine. In either case, Eq. 14 indicates that $C \to 0$ logarithmically when $r \to \infty$; thus, no axial current is carried to infinity, which is a requisite for physically realizable flows if we do not wish protostars

to become electrically charged on a macroscopic scale. This constraint provides another reason to prefer wind solutions to breeze solutions.

In the same asymptotic limit, the nondimensional density becomes

$$\rho \to \frac{C}{\beta r^2 \sin^2\theta}; \tag{17}$$

whereas the dimensionless wind velocity in an inertial frame acquires the magnitude

$$\mathrm{v_w} \to (2J - 3 - 2C\beta)^{1/2}. \tag{18}$$

The term $2C\beta$ on the right-hand side represents the usual magnetic-field correction to the terminal velocity, since $C\beta = -\varpi B_\varphi \mathbf{B}\cdot\hat{\mathbf{n}}/\rho\mathbf{u}\cdot\hat{\mathbf{n}} \equiv J_B$ is the ratio of the Maxwell torque of the field to the mass flux carried by the gas in any direction $\hat{\mathbf{n}}$. If $C \to 0$ when $r \to \infty$, the terminal velocity on every streamline achieves its maximum theoretical value $(2J-3)^{1/2}$ at infinity, as previously quoted for the averaged behavior.

Except for the slow r dependence of C and the moderate θ dependence of $\beta(\psi)$, the velocity field behaves as an angle-dependent radial wind, while the density has the distribution of a cylindrical jet, with $\rho \propto 1/\varpi^2$. Note also that $B_\varphi = \beta\rho u_\varphi \to -\varpi\beta\rho$, since at large ϖ the wind rotates hardly at all and the magnetic field wraps azimuthally at a rate governed by the rotation of its footpoint, combined with the outward sweep of the wind. With Eq. (17), we have $B_\varphi \to -C(r)/r\sin\theta$, which demonstrates that, within a scaling constant, C is the axial current carried in the X-wind flow. Because C is only a function of r, the asymptotic structure of the do- minant magnetic field component has no associated θ-component of Lorentz force:

$$-\frac{B_\varphi}{r\sin\theta}\frac{\partial}{\partial\theta}(B_\varphi\sin\theta) = 0, \tag{19}$$

independent of the exact variation of C with r. In other words, the solution of the BE and GSE asymptotically requires a balance of magnetic tension and magnetic pressure forces in the θ direction. A logarithmically slow collimation of streamlines does occur as field lines (and therefore streamlines) are pushed toward the rotational axis by the magnetic stress balance with the declining magnetic pressure of the hollow cone. Stated differently, the inner portions of X-winds collimate into jets because their hollow axial cores cannot expand enough to defocus the flow.

Shang and Shu (1999) developed a semi-analytic interpolation method to reconstruct the solution of the X-wind for the scales of observational interests, which combines the analytic solutions for the near- and far-regimes. In particular, the treatment includes a self-consistent prescription of the mass loading onto magnetic fields and the specific angular momentum carried on each streamline that allows smooth passage through the three critical surfaces (slow-MHD, Alfvén, and fast-MHD) possessed by "wind solutions." The results are in acceptable agreement with the numerical solutions of Najita and Shu (1994) in the intermediate sub-Alfvénic regime.

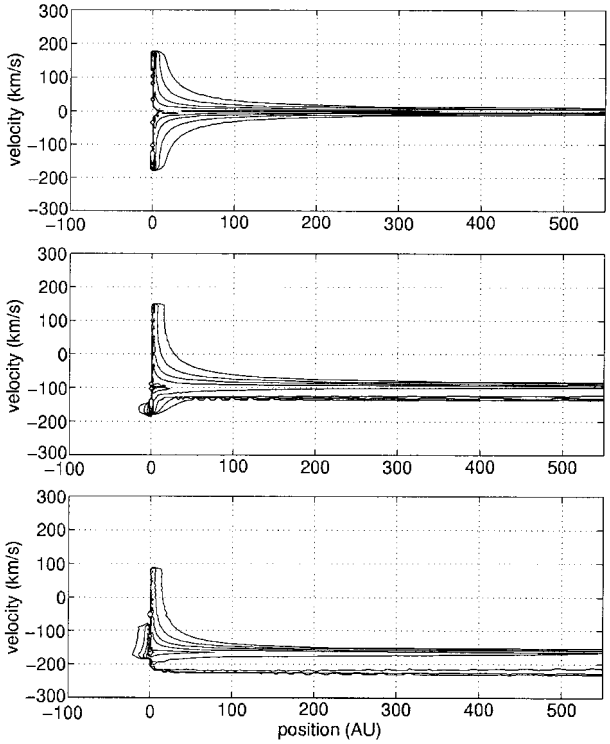

Figure 4. Position-velocity diagrams for [S II]λ6731 emission. The different figures correspond to inclination angles i=90° (*top*), 60° (*middle*), and 30° (*bottom*). Each contour level for I_λ differs by $\sqrt{10}$ from the adjacent level. See the caption for Fig. 3 in Shang *et al.* (1998).

Using such a scheme of modeling, Shang *et al.* (1998) constructed synthetic images and long-slit spectra of steady-state X-winds in the forbidden [S II]λ6716/6731 and [O I]λ6300/6364 lines with which jets are often observed. Assuming constant temperature and ionization fraction, they adopted non-LTE five-level atomic models for [S II] and [O I]. In agreement with real astronomical images (except for the knotty appearance), the isophotal contours appear highly collimated because of the strong cylindrical density stratification produced by magnetic effects (see Figs. 1 and 2 in Shang *et al.*, 1998). The kinematic information that a radially directed space-filling wide-angle wind is actually present can best be extracted from long-slit spectra taken along the jet axis. The combination of smooth acceleration and projection of multi-directional velocity vectors along the line of sight produces a wide line-profile at the base of the flow that spans large negative to large positive speeds (typically -200 to $+100$ km/s). This feature distinguishes X-winds from all pure jet models. Progressing up the jet axis, the line profile narrows to straddle the projected terminal velocity of a highly collimated flow (see Fig. 4). A narrow range of terminal velocities here is indicative that the base of the flow spans a narrow range of disk radii, a feature of X-winds but not disk winds. These qualitative and quantitative agreements between synthetic and real images/long-slit spectra reinforce the view that X-winds constitute the best current theoretical explanation for YSO jets and outflows.

5. Formation of Chondrules and CAIs

We envision the following connection between X-winds and CAIs. Imagine the accretion flow of gas and dust through a YSO disk. The dust in the disk is self-shielded from the direct rays of the Sun and is relatively cool. Either through cold

sticking or through flash melting by flares once they approach the primitive Sun closely enough, the dust aggregates inside the disk become the precursors of chondrules and CAIs. When the accreting material arrives at the stellar magnetopause at the X-point, a fraction f of the gas is launched from the inner edge of the disk at R_X as an X-wind. A fraction f roughly of the precursor rocks is also lifted with the gas into the wind by strong gas-grain coupling in the X-region. Pulled out of the shade of the disk and exposed to full sunlight at a typical distance of 10 to 20 times the present radius of the Sun, they are heated to high temperatures for days. If heated to above $\sim$1700 K for such periods of time, only the most refractory material could survive the flight and re-enter the disk as CAIs.

For petrographical reasons and because of their partial retention of moderate volatiles, chondrules require much briefer periods of being raised to melting temperatures for their generation and survival. Indeed, the time to completely evaporate a droplet of silicate melt in a vacuum is

$$t_{\rm evap} = \frac{\rho_{\rm c} R_{\rm c}}{P_{\rm V}(T)} \left(\frac{\pi k T}{2m} \right)^{1/2} , \tag{20}$$

where $P_{\rm V}(T)$ is the vapor pressure, $\rho_{\rm c}$ and $R_{\rm c}$ are the internal density and radius of the (molten) chondrule, T is the temperature, k is the Boltzmann constant and m is the mean molecular mass of the gaseous phase of the melt. Shu *et al.* (1996) estimated that chondrules can only stay molten for a few hours before they evaporate completely. To try to explain how chondrules can survive longer flights in the X-wind, they invoked equatorial heating of rotating, fluffy, dustballs to reach local melting temperatures for only seconds when the mean solar radiation field is too weak to melt and evaporate chondrules as a whole. This artifice was convincing to no one, not even ultimately to the authors themselves.

Fortunately, observed YSOs have sources of intense energy release other than sunlight, and Shu *et al.* (1997) considered the possibility of briefer heating events in the more complex context of a fluctuating X-wind model. In particular, flash heating of primitive rocks by the light (at optical to *X*-ray wavelengths) or energetic particles released by impulsive solar flares is a promising mechanism for producing chondrules. Deeper in the reconnection ring, where the flare events are more intense, they may even provide a way to repeatedly evaporate protoCAIs, putting their solids into a hot gaseous state, and then recondensing them out as solids again from the vapor. The absence of mass-dependent isotopic fractionations make some CAIs better explained as gaseous condensates than as evaporative residues, contrary to the pure radiative heating model of Shu *et al.* (1996; see also Sect. 6 below). On the other hand, other type A and B CAIs, which show evidence of mass-dependent, isotopic mass fractionation in Mg, may have a contribution of evaporative residues from radiative heating in the X-wind, as in Shu *et al.* (1996).

After launch in the wind, chondrules will cool below their Curie points, and their ferromagnetic components will record the ambient magnetic field strength. According to our fiducial models (Shu *et al.*, 1996; 1997), the impressed magnetic

fields would have intensities of 0.09–0.3 mT in the fiducial cases, in rough agreement with measured values (Sugiura and Strangway, 1988). Launch in the X-wind would allow these materials to be thrown out from the inner edge of the disk to interplanetary distances, where they can be incorporated into the parent bodies of chondritic meteorites, after having recorded the magnetic field of the primitive Sun.

6. Numerical Examples and Radiative Heating

To illustrate the ideas more quantitatively, consider two fiducial numerical examples of the main evolutionary stages of low-mass star formation. The first example represents the early stage when the young star is still deeply embedded inside its infalling envelope of gas and dust; the second, the later stage when the star and the disk have been revealed as optical and infrared objects (Shu *et al.*, 1987; 1997). The parameters for the embedded stage are $M_* = 1 \times 10^{33}$ g, $R_* = 2.1 \times 10^{11}$ cm, $R_X = 4\ R_*$, and $\dot{M}_w = 3 \times 10^{19}$ g/s. The embedded stage lasts for about 2×10^5 years. The parameters for the revealed stage are $M_* = 1.6 \times 10^{33}$ g, $R_* = 2.1 \times 10^{11}$ cm, $R_X = 5.3\ R_*$, and $\dot{M}_w = 2 \times 10^{18}$ g/s. The revealed stage lasts for about 3×10^6 years.

The above numbers have been chosen to agree approximately with the empirical results of many observational groups. However, no quantitative Zeeman measurements exist to estimate the magnetic dipole moments μ_* of the central stars in deeply embedded sources. To obtain the value of R_X in these circumstances, we suppose that although protostars may have stronger dynamos than T Tauri stars, any increase in μ_* for them is more than offset by their larger disk accretion rates $\dot{M}_D$. Thus, we adopt the hypothesis that R_X has a secular trend to increase with evolutionary time, roughly as the stellar mass M_* itself increases.

In the protosolar radiation field, the surface-averaged radiative-equilibrium temperature of a CAI or chondrule is

$$\bar{T}_{eq} = \left[\mathcal{F}_{D*} \frac{L_* \exp(-\tau_*)}{16\pi\sigma r^2} + \frac{\mathcal{E}}{a} \right]^{1/4}, \tag{21}$$

where $\mathcal{F}_{D*}$ is the fraction of the star's of luminosity L_* unocculted by the disk with a hole in it when measured at a distance r, τ_* is the average optical depth associated with material along the line of sight to unocculted parts of the stellar photosphere, $\mathcal{E}$ is the diffuse radiation field present in the problem, σ is the Stefan-Boltzmann constant, and a is the radiation constant. In the above equation, we have ignored viscous effects near the inner edge of the disk and a small term associated with the aerodynamic heating of the X-wind (Shu *et al.*, 1996). Inside the disk at R_X, τ_* is essentially infinite, and the diffuse radiation field $\mathcal{E} = aT_X^4$ is that of a blackbody at temperature T_X given by Adams *et al.* (1987)

$$T_X = \left\{ \frac{L_*}{4\pi^2\sigma R_*^2} \left[\sin^{-1}\left(\frac{R_*}{R_X}\right) - \left(\frac{R_*}{R_X}\right)\left(1 - \frac{R_*^2}{R_X^2}\right)^{1/2} \right] \right\}^{1/4}. \tag{22}$$

Thus, inside the disk, $\bar{T}_{\rm eq} = T_{\rm X}$. Above the disk, $\mathcal{E}$ can be approximately estimated to be half of a blackbody at the temperature $T_{\rm X}$, $\mathcal{E} = aT_{\rm X}^4/2$. When a CAI or chondrule is lifted out of the disk, the maximum surface-averaged temperature that it can reach is given by the assumptions, $\mathcal{F}_{\rm D*} = 1$ and $\tau_* = 0$, *i. e.*,

$$\bar{T}_{\rm peak} = \left[\frac{L_*}{16\pi\sigma R_{\rm X}^2} + \frac{1}{2}T_{\rm X}^4\right]^{1/4}. \tag{23}$$

Bodies lofted by the X-wind experience temperatures close to the peak typically for a few days, while their radial distances from the Sun increase from $\sim$1.0 to $\sim$1.5 $R_{\rm X}$. When $R_{\rm X}$ begins very small, no solid matter can survive this direct sunlight heating. As $R_{\rm X}$ increases systematically with protostellar evolutionary time, CAIs can survive the flight; and later, chondrules. The base and peak temperatures, $(T_{\rm X}, T_{\rm peak})$ for the fiducial embedded and revealed cases are (1200 K, 1800 K) and (800 K, 1300 K), respectively. The first value for $T_{\rm peak}$, 1800 K, is high enough to melt most rocky materials, but the second, 1300 K, is not. The inferred cooling rates along the trajectories in a direct radiation field are $> 3^\circ$/hr in the embedded phase and $> 2^\circ$/hr in the revealed phase. We conclude that CAIs can be formed by direct heating via sunlight during the embedded stages of protostellar evolution; in the revealed stages, CAI formation will be rarer. Perhaps this distinction explains the difference between carbonaceous chondrites, which possess plentiful CAIs, with most being large; and ordinary chondrites, possessing few CAIs, with any present being small.

In contrast, the formation of chondrules must occur by more transient flare-heating events. Moreover, for such flare-heated objects to survive later exposure to full sunlight, launch in the X-wind must either occur during the revealed stage of YSO evolution, or during a fluctuation when $R_{\rm X}$ has a substantially larger value than the average adopted for our fiducial embedded-stage example.

Shu *et al.* (1997) gave some examples of fluctuating X-wind models that could satisfy the meteoritic constraints. The embedded phase in their examples have base temperatures in the range 750 K$< T_{\rm X} <$1600 K, the revealed phase in the range 500 K $< T_{\rm X} <$1100 K. The peak temperature fluctuates between 1300 K and 2200 K in the embedded phase, and between 950 K and 1600 K in the revealed phase. Therefore, in the low magnetic and average states, $T_{\rm X}$ is high enough to drive out most of the FeS, Na, and K originally contained in the chondrule precursors. When launched, the rocks remain near peak temperatures for days. During this time, extensive evaporation occurs, leaving a residue that becomes molten or partially molten CAIs. On the other hand, in the high states of the revealed phase, $T_{\rm X}$=500 K is low enough to retain volatiles in the chondrule precursors; during flight the peak temperature reached is insufficient to completely melt the magnesium-iron silicates, and the rocks can partially retain Na and K. The production of chondrules during high magnetic states may be mixed with the production of CAIs in low magnetic states in alternate decades.

These examples are illustrative only, and it could be that future developments will show that we have over-estimated the base temperatures in the X-region by ignoring the albedo of chondules and CAIs. A nonzero albedo will reflect some of

the light shining on the solids rather than allowing it all to be absorbed. There may be other radiative-transfer effects that we've neglected in our estimates for T_X and T_{peak} that would make quibbles about a few hundred K, up or down (which are important for many geochemical considerations), meaningless. The more important issue may be the timescales of the heating events that give rise to chondrules.

7. Flash Heating and Size Sorting

Observations of *X*-ray flares in YSOs show very fast rise times, followed by a slower decay of tens of minutes to a few hours. Heating by optical or *X*-ray photons released by large flares in the helmet streamer can double or triple the base temperatures T_X because of the favorable illumination geometry (see Fig. 3). Heating by solar energetic particles accelerated by flares in the helmet streamer or reconnection ring may be even more efficient because the magnetic field lines of these configurations always focus a fraction of the charged particles down to the footpoints near the X-region where protoCAIs and protochondrules are to be found.

The process by which X-winds will automatically size-sort the material that re-enters the disk is straightforward. The result depends mainly on the numerical value of a dimensionless coupling constant associated with gas-solid drag:

$$\alpha \equiv \frac{3C_D\dot{M}_w}{16\pi\,(GM_*R_X)^{1/2}\rho_c R_c}, \tag{24}$$

where C_D is a drag coefficient of unity, and ρ_c and R_c are again the density and radius of the spherical body of rock. Large bodies with small values of α are poorly coupled to the X-wind and crash back into the disk not far from the launch point, where they are eventually swept into the Sun by the general accretion flow. Small rocks with large values of α are well coupled to the gas flow and carried by the X-wind to interstellar space. Only a narrow range of moderately sized rocks, with α in the range of 0.2–0.3 for the median streamline, are coupled sufficiently to the X-wind that they can be thrown to interplanetary but not infinite distances on an inclined elliptic orbit that reintersects the disk. These become the chondrules and CAIs of chondritic meteorites. Small fragments can smash into the surface of a gently flared disk at hyperbolic speeds and be stopped there, and they may become the igneous materials that comprise a part of the matrix of all chondritic meteorites. Even CI chondrites, which lack large CAIs or chondrules, are not comprised entirely of pristine presolar grains.

For the value $\alpha \approx 0.25$, where the median streamline of the model of Shang and Shu (1999) sprays particles to the asteroid belt, the particle diameters are 3.0 and 0.14 mm for the high magnetic states, and 4.9 and 0.22 mm for the low magnetic states of the embedded and revealed phases, respectively. These sizes compare well with the chondrules and CAIs found in chondrites. Accounting for launch from different streamlines and for fluctuations within magnetic cycles will probably not add to the dispersion in sizes at any given radius in the disk by more than a factor of about 2 on both sides of the median value. Rapid and local incorporation into plan-

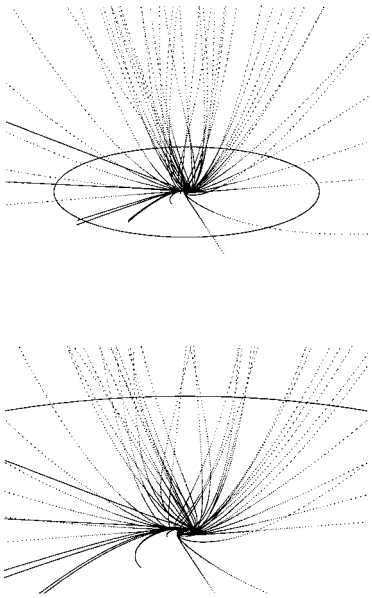

Figure 5. A 3-D visualization of trajectories of gas and dust in an X-wind. *Top:* 3-D view of trajectories of gas (*dotted lines*) launched in an X-wind from the inner edge of an accretion disk. The gas streamlines eventually collimate into a jet oriented perpendicularly to the disk, whose plane is indicated by the tilted big circle of radius 60 R_X, which is about the size of the Earth's orbit about the sun. *Bottom:* Close-up view of trajectories of rocks (*solid black lines*) carried out of the disk by the X-wind. Two black lines are drawn for each trajectory: the upper one depicts the actual three-dimensional motion; the lower one shows the shadow cast by the trajectory if it were illuminated from above. The vertical separation between the trajectory and its shadow is the height of the rock above the midplane of the thin disk. Large rocks (shortest curved trajectory, $\alpha \approx 0.1 - 0.23$) crash back into the disk before getting very far from the launch point. Small rocks (longest and straightest trajectory, $\alpha \approx 1$) are well coupled to the gas and are carried to interstellar space by the X-wind.

etesimals of CAIs and chondrules produced during any epoch will then preserve the narrow re-entry size-distribution. Since the spray of CAIs and chondrules occurs at all radii in the solar nebula, the X-wind theory predicts that such igneous rocks should be found, not only in undifferentiated (parts of) asteroids, but also in comets. We eagerly await the results from proposed comet-sample return missions.

8. Protosolar Cosmic Rays and Extinct Radioactivities

The X-wind environment also possesses the potential of producing some of the extinct radionuclides inferred for meteorites through the bombardment of proto-CAIs and -chondrules by solar cosmic rays (Lee *et al.*, 1998). In particular, irradiation within the solar system to produce the shortest-lived radioactivities, such as ^{41}Ca, ^{26}Al, and ^{53}Mn, may resolve the difficulties faced by attempts to make these isotopes by external stellar seeding just before the protosolar cloud collapsed. Galactic nucleosynthesis can maintain steady-state levels of the longer-lived species, ^{107}Pd, ^{129}I, ^{244}Pu, and ^{146}Sm at or above the meteoritic levels (Clayton and Jin, 1995).

In addition to the problem of overall energetics involved with irradiating rocks at the distance of the asteroid belt, the usual approach to this problem encounters a severe difficulty because it is based (*e. g.*, Vanhala and Goswami, 2000) on satellite observations of solar energetic particles accelerated in gradual flares: The total fluence of their dominant particles, protons and alphas, sufficient to synthesize meteoritic levels of ^{41}Ca and ^{53}Mn falls short by a factor of 20 to produce enough ^{26}Al. Hence, a novel reaction pathway is needed to resolve this discrepancy.

Lee *et al.* (1998) found a resolution of the difficulty within the context of the fluctuating X-wind model. On the modern Sun, gradual flares (CMEs) dominate the

TABLE I
Production in X-wind Local Irradiation Model.

N_R/N_S	^{3}He	p and α	Major Reaction
^{26}Al/^{27}Al	5×10^{-5}	–	^{24}Mg(^{3}He,p)^{26}Al
	–	2.5×10^{-6}	^{27}Al(p,pn)^{26}Al, etc.
^{41}Ca/^{40}Ca	2.6×10^{-6}	–	^{40}Ca(^{3}He,2p)^{41}Ca
	–	1.5×10^{-8}	^{42}Ca(p,pn)^{41}Ca
^{53}Mn/^{55}Mn	–	3.0×10^{-5}	^{56}Fe(p,α/2p2n)^{53}Mn
^{138}La*/^{139}La	–	6.6×10^{-6}	^{138}Ba(p,n)^{138}La
^{50}V*/^{51}V	7.4×10^{-6}	7.5×10^{-6}	^{48}Ti(^{3}He/α,p/pn)^{50}V

solar output of cosmic rays that reach interplanetary space because these CMEs occur high in the solar corona on open field lines. Collisionless shockwaves associated with the CMEs efficiently accelerate protons and alphas, but not electrons. Impulsive flares occurring by reconnection events on closed field lines lower in the solar corona appear roughly 10 times more frequently than gradual flares, and they give more spectacular light displays because their accelerated particles are rich in electrons. Even more important for our discussion in this section, the energetic particle spectrum of impulsive flares is also rich in ^{3}He ions, probably as a result of acceleration by wave-particle resonances exceptionally favorable to ^{3}He nuclei because of its unique charge-to-mass ratio (which gives it a gyrofrequency intermediate to that of protons and alphas; Temerin and Roth, 1992; Roth and Temerin, 1997).

If YSOs behave as does the modern Sun, then impulsive flares arising from the reconnection ring are a prolific source of ^{3}He cosmic rays. At energies of 1 MeV/amu or larger, the most favorable for nuclear reactions, they may have numbers in excess of alphas and comparable to protons. The exothermic reaction ^{24}Mg(^{3}He,p)^{26}Al can then yield the canonical abundance ^{26}Al/^{27}Al of 5×10^{-5} for reasonable conversion factors of hard *X*-rays observed from protostars, which arise by bremmstrahlung from energetic electrons, to the associated energetic ions. Moreover, the protons and alphas that go along with the ^{3}He needed to make ^{26}Al correctly produce the observed meteoritic levels of ^{41}Ca and ^{53}Mn. Unfortunately, if ^{40}Ca(^{3}He,2p)^{41}Ca is added in the reaction, ^{41}Ca is overproduced by a factor of $\sim$200 (see Tab. I).

There may be a way out of this difficulty. To explain the correct production of ^{26}Al by ^{3}He bombardment of ^{24}Mg in the first place, it is necessary to postulate that protoCAIs possess cosmic levels of ^{24}Mg relative to ^{27}Al. This postulate is sensible in the context of the fluctuating X-wind picture only if repeated flare events evaporate and redeposit thick mantles of magnesium-rich minerals on top of calcium-aluminum-rich cores. The ^{24}Mg-rich mantle would make an accessible target for the ^{3}He synthesis of ^{26}Al, but they would stop the same MeV ^{3}He particles before they could penetrate to the ^{40}Ca-rich core to make ^{41}Ca. Upon launch in the X-wind, the heated ^{26}Al would diffuse into the refractory core, whereas the

magnesium (and iron) rich mantle would evaporate away (just as chondrules do), leaving only the relatively thin rims that are found surrounding most CAIs today.

This proposal, as it was originally made by Shu *et al.* (1997) and Lee *et al.* (1998), sounds fairly ad hoc. Nevertheless, Krot *et al.* (1999) have since found in CH meteorites examples of CAIs coated by exactly the type of thick chondrule mantles that would make the proposal work. Moreover, such CAIs contain no measurable levels of extinct ^{26}Al (McKeegan, pers. commun.), which is expected if they were launched at a sufficiently large distance from the young Sun that their chondrule-like mantles did not evaporate. Additional support comes from an earlier observation of CAIs with thick chondrule-like mantle made first by Bischoff and Keil (1984) in H3 ordinary chondrite Sharps. The magnesium isotopic composition of hibonite in the CAI also showed no ^{26}Mg excess (Srinivasan and Bischoff, 1998).

In these two cases, they were probably launched (with a probability of $f \sim 1/3$) without ever entering the reconnection ring, and therefore without ever being irradiated by a large fluence of ^{3}He cosmic rays. These ^{26}Al-free CAIs would then share a feature in common with FUN and UN CAIs, which Lee *et al.* (1998) also conjectured were launched by the X-wind without ever having entered the reconnection ring. Whether one accepts these explanations or not, the observations of Bischoff and Keil (1984), Misawa and Fujita (1994), Srinivasan and Bischoff (1998), Krot *et al.* (1999), Maruyama *et al.* (1999), and Russell and Kearsley (1999) strongly suggest that CAIs and chondrules have a common place of origin. This site, we claim, is in the energetic environment close to the source of the X-winds.

References

Adams, F. C., Lada, C. J., and Shu, F. H.: 1987, 'Spectral Evolution of Young Stellar Objects', *Astrophys. J.* **312**, 788–806.

Bally, J., and Lada, C. J.: 1983, 'The High-velocity Molecular Flows Near Young Stellar Objects', *Astrophys. J.* **265**, 824–847.

Bieging, J. H., Cohen, M., and Schwartz, P. R.: 1984, 'VLA Observations of T Tauri Stars. II - A Luminosity-limited Survey of Taurus-Auriga', *Astrophys. J.* **282**, 699–708.

Bischoff, A., and Keil, K.: 1984, 'Al-rich Objects in Ordinary Chondrites – Related Origin of Carbonaceous and Ordinary Chondrites and Their Constituents', *Geochim. Cosmochim. Acta* **48**, 693–709.

Blandford, R. D.: 1976, 'Accretion Disk Electrodynamics – A Model for Double Radio Sources', *Mon. Not. Roc. Astro. Soc.* **176**, 465–481.

Blandford, R. D., and Payne, D. G.: 1982, 'Hydromagnetic Flows From Accretion Disks and the Production of Radio Jets', *Mon. Not. Roc. Astro. Soc.* **199**, 883–903.

Bok, B. J.: 1978, 'Star Formation in or Very Close to a Southern Globule', *Pub. Astron. Soc. Pac.* **90**, 489–490.

Bührke, T., Mundt, R., Ray, T. P.: 1988, 'A Detailed Study of HH 34 and its Associated Jet', *Astron. Astrophys.* **200**, 99–119.

Cabrit, S., Bertout, C.: 1992, 'CO Line Formation in Bipolar Flows – III. The Energetics of Molecular Flows and Ionized Winds', *Astron. Astrophys.* **261**, 274–284.

Clayton, D. D., and Jin, L.: 1995, 'Gamma Rays, Cosmic Rays, and Extinct Radioactivity in Molecular Clouds', *Astrophys. J.* **451**, 681–699.

Cudworth, K. M., and Herbig, G. H.: 1979, 'Two Large-proper-motion Herbig-Haro Objects', *Astron. J.* **84**, 548–551.

Edwards, S., and Snell, R. L.: 1982, 'A Search for High-velocity Molecular Gas Around T Tauri Stars', *Astrophys. J.* **261**, 151–160.
Fukui,Y., Iwata,T., Mizuno,A., Bally,J., and Lane,A.P.: 1993, 'Molecular Outflows', *in* E.H. Levy and J.I. Lunine (eds.), *Protostars and Planets III*, Univ. Arizona Press (UAP), Tucson, pp. 603–639.
Giovanardi, C., Lizano, S., Natta, A., Evans, N. J. II, and Heiles, C.: 1992, 'Neutral Winds From Protostars', *Astrophys. J.* **397**, 214–224.
Ghosh, P., and Lamb, F. K.: 1979a, 'Accretion by Rotating Magnetic Neutron Stars. II - Radial and Vertical Structure of the Transition Zone in Disk Accretion', *Astrophys. J.* **232**, 259–276.
Ghosh, P., and Lamb, F. K.: 1979b, 'Accretion by Rotating Magnetic Neutron Stars. III - Accretion Torques and Period Changes in Pulsating *X*-ray Sources', *Astrophys. J.* **234**, 296–316.
Ghosh, P., Pethick, C. J., and Lamb, F. K.: 1976, *Astrophys. J.* **217**, 578.
Glassgold,A.E., Feigelson,E.D., and Montmerle,T.: 2000, '*Effects of Energetic Radiation in YSOs*', *in* V. Mannings, A.P. Boss, and S.S. Russell (eds.), *Protostars and Planets IV*, UAP, in press.
Haro, G. 1952, *Astrophys. J.*, **115.**, 572
Haro, G. 1953, *Astrophys. J.* **117**, 73.
Hayashi, M.R., Shibata, K., and Matsumoto, R.: 1996, '*X*-Ray Flares and Mass Outflows Driven by Magnetic Interaction Between a Protostar and Its Surrounding Disk', *Astrophys. J.* **468**, L37–L40.
Herbig, G. H.: 1950, *Astrophys. J.* **111**, 11.
Herbig, G. H.: 1951, *Astrophys. J.* **113**, 697.
Königl, A., and Pudritz, R. E.: 2000, 'Disk Winds and the Accretion-Outflow Connection', *in* V. Mannings, A. P. Boss, and S. S. Russell, *Protostars and Planets IV*, UAP, in press.
Knapp, G. R., Kuiper, T.B.H., Knapp, S. L., and Brown, R. L. 1976, 'CO Observations of NGC 1579 /S222/ and S239', *Astrophys. J.* **206**, 443–451.
Krot, A. N., Weber, D., Greshake, A., Ulyanov, A. A., MCKeegan, K. D., Hutcheon, I., Sahijpal, S., and Keil, K.: 1999, 'Relic Ca,Al-rich Inclusions in Chondrules From the Carbonaceous Chondrites ACFER 182 and ACFER 094', *Lunar and Planetary Sci. Conf.* **30**, # 1511 (abstract).
Lada, C. J.: 1985, 'Cold Outflows, Energetic Winds, and Enigmatic Jets Around Young Stellar Objects', *Ann. Rev. Astron. Astrophys.* **23**, 267–317.
Lee, T., Shu, F. H., Shang, H., Glassgold, A. E., and Rehm, K. E.: 1998, 'Protostellar Cosmic Rays and Extinct Radioactivities in Meteorites', *Astrophys. J.* **506**, 898–912.
Linker, J. A., and Mikić, Z.: 1995, 'Disruption of a Helmet Streamer by Photospheric Shear', *Astrophys. J.* **438**, L45–L48.
Lizano, S., Heiles, C., Rodriguez, L. F., Koo, B.-C., Shu, F. H., Hasegawa, T., Hayashi, S., Mirabel, I. F.: 1988, 'Neutral Stellar Winds that Drive Bipolar Outflows in Low-mass Protostars', *Astrophys. J.* **328.**, 763–776.
Lovelace, R.V. E.: 1976, 'Dynamo Model of Double Radio Sources', *Nature* **262.**, 649–652.
Margulis, M., and Lada, C. J.: 1985, 'Masses and Energetics of High-Velocity Molecular Outflows', *Astrophys. J.* **299**, 925–938.
Maruyama, S., Yurimoto, H., and Sueno, S.: 1999, 'Spinel-Bearing Chondrules in the Allende Meteorite', *Meteoritics and Planet. Sci.* **32**, A98.
Mestel, L.: 1968, *Mon. Not. Roy. Astron. Soc.* **138**, 359.
Meyer, M. R., Calvet, N., and Hillenbrand, L. A.: 1997, 'Intrinsic Near-Infrared Excesses of T Tauri Stars: Understanding the Classical T Tauri Star Locus', *Astron. J.* **114.**, 288–300.
Misawa, K., and Fujita, T.: 1994, 'A Relict Refractory Inclusion in a Ferromagnesian Chondrule From the Allende Meteorite', *Nature* **368**, 723–726.
Mundt, R., and Fried, J. W.: 1983, 'Jets From Young Stars', *Astrophys. J.*, **274.**, L83.
Mundt, R., Bührke, T., Fried, J. W., Neckel, T., Sarcander, M., and Stocke, J.: 1984, 'Jets From Young Stars III. The Case of Haro 6-5B, HH 33/40, HH 19, and 1548C27', *Astron. Astrophys.* **140**, 17–23.
Mundt, R., Brugel, E. W., and Bührke, T.: 1987, 'Jets From Young Stars - CCD Imaging, Long-slit Spectroscopy, and Interpretation of Existing Data', *Astrophys. J.* **319**, 275–303.
Najita, J. R., and Shu, F. H.: 1994, 'Magnetocentrifugally Driven Flows From Young Stars and Disks. 3: Numerical Solution of the Sub-Alfvenic Region', *Astrophys. J.* **429**, 808–825.

Ostriker, E. C., and Shu, F. H.: 1995, 'Magnetocentrifugally Driven Flows From Young Stars and Disks. IV. The Accretion Funnel and Dead Zone', *Astrophys. J.* **447**, 813–828.
Poetzel, R., Mundt, R., and Ray, T. P.: 1989, 'Z CMa – A Large-scale High Velocity Bipolar Outflow Traced by Herbig-Haro Objects and a Jet', *Astron. Astrophys.*, **224**, L13–L16.
Reipurth,B.:1989,'The HH111 Jet and Multiple Outflow Episodes From Young Stars', *Nature* **340**, 42.
Rodríguez, L. F., Lizano, S., Cantó, J., Escalante, V., and Mirabel, I. F.: 1990, 'VLA Observations of High-velocity H I Associated With the Herbig-Haro Objects 7-11', *Astrophys. J.* **365**, 261–268.
Rodríguez, L. F., Moran, J. M., and Ho, P.T.P. 1980, 'Anisotropic Mass Outflow in Cepheus A', *Astrophys. J.* **240**, L149–L152.
Roth, I., and Temerin, M.: 1997, 'Enrichment of ^{3}He and Heavy Ions in Impulsive Solar Flares', *Astrophys. J.* **477**, 940–957.
Ruiz, A., Alonso, J. L., and Mirabel, I. F.: 1992, 'Possible Detection of a High-velocity Neutral Wind in T Tauri', *Astrophys. J.* **394**, L57–L59.
Russell, R. W., and Kearsley, A. T.: 1999, *Meteoritics and Planet. Sci.* **34**, Suppl., A99.
Shang, H., and Shu, F. H.: 1999, *Astrophys. J.*, in preparation.
Shang, H., Shu, F. H., and Glassgold, A. E.: 1998, 'Synthetic Images and Long-slit Spectra of Protostellar Jets', *Astrophys. J.* **493**, L91–L94.
Shu, F. H.: 1995, *in* C. Yuan and J. You (eds.), *Molecular Clouds and Star Formation*, World Scientific, Singapor, p. 97.
Shu, F. H., Adams, F. C., and Lizano, S.: 1987, 'Star Formation in Molecular Clouds – Observation and Theory', *Ann. Rev. Astron. Astrophys.* **25**, 23–81.
Shu, F., Najita, J., Ostriker, E., Wilkin, F., Ruden, S., and Lizano, S. 1994a, 'Magnetocentrifugally Driven Flows From Young Stars and Disks. 1: A Generalized Model', *Astrophys. J.* **429**, 781–796.
Shu, F.H., Najita, J., Ruden, S., and Lizano, S. 1994b, 'Magnetocentrifugally Driven Flows From Young Stars and Disks. 2: Formulation of the Dynamical Problem', *Astrophys. J.*, **429**, 797–807.
Shu, F. H., Najita, J., Ostriker, E., and Shang, H.: 1995, 'Magnetocentrifugally Driven Flows from Young Stars and Disks. V. Asymptotic Collimation into Jets', *Astrophys. J.* **455**, L155–L158.
Shu, F. H., Shang, H., and Lee, T.: 1996, 'Toward an Astrophysical Theory of Chondrites', *Science* **271**, 1545–1552.
Shu, F. H., Shang, H., Glassgold, A. E., and Lee, T.: 1997, '*X*-rays and Fluctuating X-winds From Protostars', *Science* **277**, 1475–1479.
Shu, F. H., Allen, A., Shang, H., Ostriker, E. C., and Li, Z.-H.: 1999, *in* C. J. Lada, *NATO-ASI Proc*.
Shu, F. H., Najita, J., Shang, H., and Li, Z.-H.: 2000, 'X-winds: Theory and Observations', *in* V. Mannings, A. P. Boss, and S. S. Russell, *Protostars and Planets IV*, UAP, in press.
Snell, R. L., Loren, R. B., and Plambeck, R. L.: 1980, 'Observations of CO in L1551 - Evidence for Stellar Wind Driven Shocks', *Astrophys. J.* **239**, L17–L22.
Strom, S., Grasdalen, G. L., and Strom, K. M.: 1974, 'Infrared and Optical Observations of Herbig-Haro objects', *Astrophys. J.* **191**, 111–142.
Stocke, J. T., Hartigan, P. M., Strom, S. E., Strom, K. M., Anderson, E. R., Hartmann, L. W., and Kenyon, S. J.: 1988, 'A Detailed Study of the LYNDS 1551 Star Formation Region', *Astrophys. J. Suppl.* **68**, 229–255.
Sugiura, N., and Strangway, D. W.: 1988, 'Magnetic Studies of Meteorites', *in* J. F. Kerridge and M. S. Matthews (eds.), *Meteorites and the Early Solar System*, UAP, pp. 595–615.
Srinivasan, G., and Bischoff, A.: 1998, 'Magnesium-Aluminum Study of Hibonites Within a Chondrule-like Object from Sharps (H3)', *Meteoritics and Planet. Sci.* **32**, A148.
Temerin, M., and Roth, I.: 1992, 'The Production of He-3 and Heavy Ion Enrichment in He-3-rich Flares by Electromagnetic Hydrogen Cyclotron Waves', *Astrophys. J.* **391**, L105–L108.
Vanhala, H. A., and Goswami, J. N.: 2000, 'Extinct Radionuclides and the Origin of the Solar System', *in* V. Mannings, A.P. Boss, and S.S. Russell, *Protostars and Planets IV*, UAP, in press.
Weidenschilling, S. J., and Cuzzi, J. N.: 1993, 'Formation of Planetesimals in the Solar Nebula', *in* E. H. Levy and J. I. Lunine (eds.), *Protostars and Planets III*, UAP, pp. 1031–1060.

Address for Offprints: Hsien Shang, Harvard-Smithsonian Center for Astrophysics, 60 Garden Street, MS-42, Cambridge, MA 02138, USA; hshang@cfa.harvard.edu